

## **Supplementary Information**

### **Rapid Synthesis of Gold Nanoparticles with Carbon Monoxide in a Microfluidic Segmented Flow System**

*He Huang<sup>a</sup>, Hendrik du Toit<sup>a</sup>, Sultan Ben-Jaber<sup>b</sup>, Gaowei Wu<sup>a</sup>, Luca Panariello<sup>a</sup>,*

*Nguyen Thi Kim Thanh<sup>c,d</sup>, Ivan P. Parkin<sup>b</sup>, Asterios Gavriilidis<sup>a</sup>*

a. Department of Chemical Engineering, University College London, Torrington Place,  
London, WC1E 7JE, United Kingdom

b. Department of Chemistry, University College London, 20 Gordon Street,  
London, WC1H 0AJ, United Kingdom

c. Biophysics Group, Department of Physics and Astronomy, University College London,  
Gower Street, London, WC1E 6BT, United Kingdom

d. UCL Healthcare Biomagnetic and Nanomaterials Laboratories, 21 Albemarle Street,  
London, W1S 4BS, United Kingdom

#### **Contents**

|   |    |
|---|----|
| 1. Experimental set-up .....  | 2  |
| 2. Comparative experiment with coiled glass tube .....                            | 3  |
| 3. Evaluation of gas-liquid mass transfer .....                                   | 4  |
| 4. Characterization of gold nanoparticles synthesized via CO reduction .....      | 6  |
| 5. Calculation of SERS enhancement factor .....                                   | 8  |
| 6. Synthesis procedures of gold nanoparticles with different capping agents ..... | 10 |

## 1. Experimental set-up

The experimental set-up with a schematic of the coiled flow inverter (CFI) reactor is shown in Figure S1. The aqueous  $\text{HAuCl}_4$  solution was combined with pure CO gas through a T-junction, and then directed to the CFI reactor. The Au nanoparticles solution was collected at the outlet of the CFI reactor.

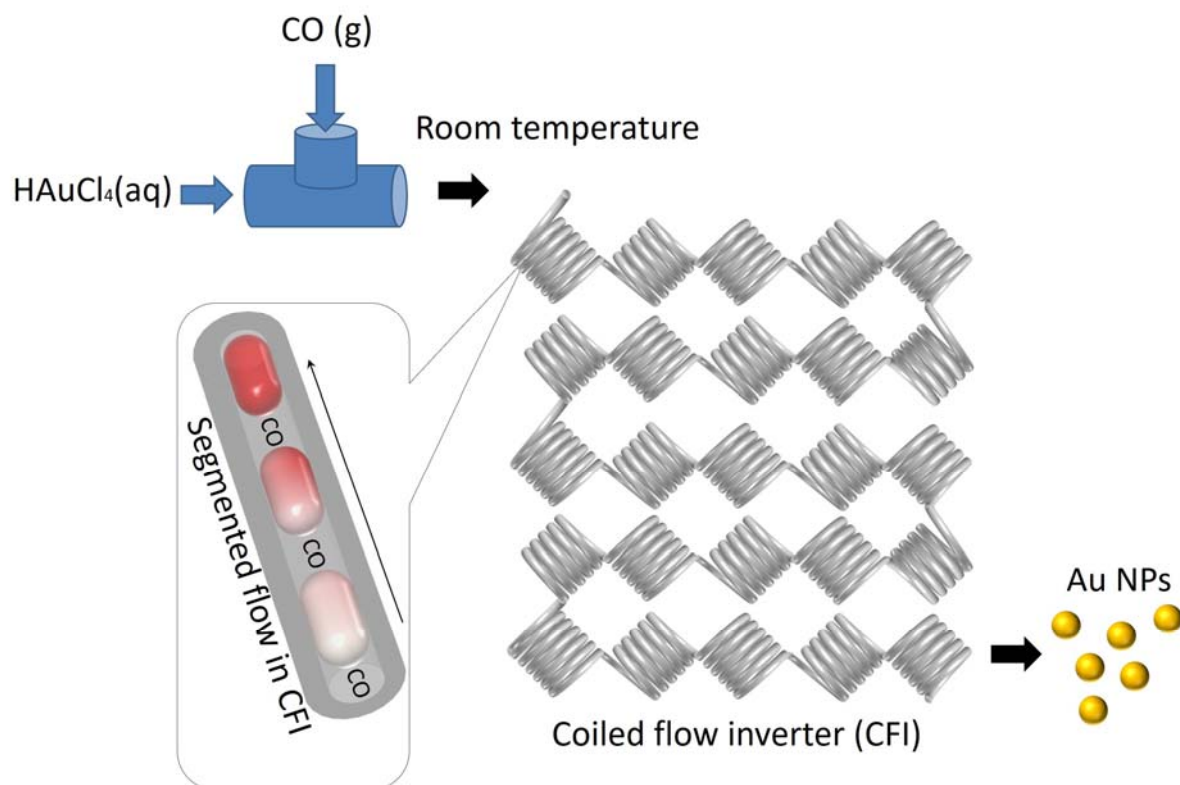


**Figure S1.** Schematic illustration of the microfluidic segmented flow system.

## 2. Comparative experiment with coiled glass tube

A coiled glass tube, without inverting the flow direction by 90°, was used for nanoparticle synthesis. Compared to the CFI reactor, the mixing performance was not as efficient due to a) the absence of 90° coil bends, b) increased inner diameter (1.5 mm vs. 1 mm), c) increased coil diameter (3 cm vs. 1 cm), d) reduced coil number (4 vs. 100), e) slower Taylor bubble velocity (0.0021 m/s vs. 0.014 m/s). Furthermore, the aqueous solution wetted the tube creating a film that may have affected the residence time distribution. The experimental conditions were the same as Figure 1b, i.e., residence time 4.4 min, inlet concentration of  $\text{HAuCl}_4$  0.27 mM and liquid to gas volumetric flow rate ratio 10. Figure S2 shows a picture of the coiled glass tube and the corresponding nanoparticle size distribution obtained from DCS. The nanoparticle size was  $7.8 \pm 1.1$  nm (14.2%), which was similar to the nanoparticles produced by the CFI ( $7.7 \pm 0.3$  nm, 4.1%). However, the polydispersity increased from 4.1% in the CFI to 14.2% in the coiled glass tube, which indicated the superior performance of the CFI for particle size distribution control.

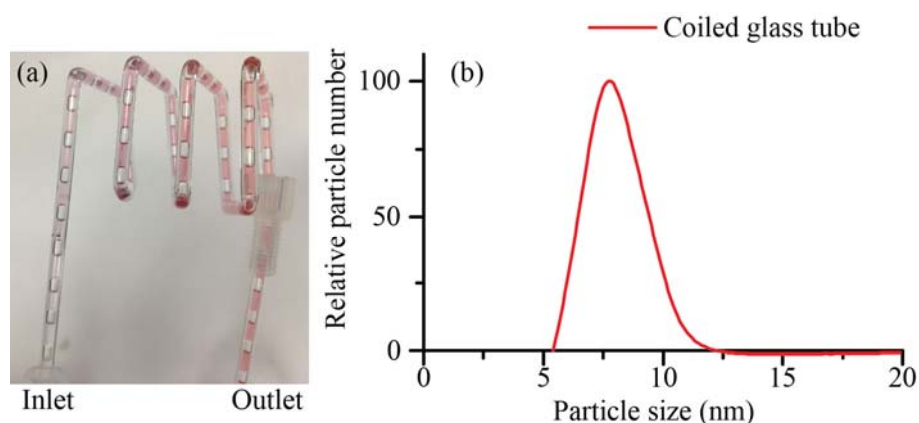


**Figure S2.** (a) Picture of coiled glass tube during nanoparticle synthesis. (b) Particle size distribution obtained from DCS (normalized by area) for CO-produced Au nanoparticles obtained at residence time 4.4 min, inlet concentration of  $\text{HAuCl}_4$  0.27 mM and liquid to gas volumetric flow rate ratio 10.

### 3. Evaluation of gas-liquid mass transfer

The flow patterns at different liquid to gas volumetric flow rate ratios are shown in Figure S3. From these, average lengths of gas bubbles and liquid slugs were estimated and shown in Table S1. In slug flow, the gas formed elongated bubbles with the same diameter as the tube, also known as Taylor bubbles.<sup>1</sup> Gas-liquid mass transfer coefficients were calculated using properties of CO and water and the set flow rates (0.5 ml/min of liquid and different liquid to gas volumetric flow rate ratios of 2 to 20).

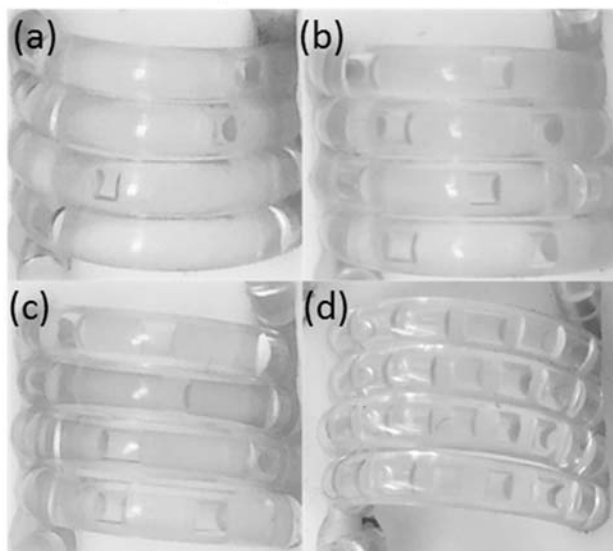


**Figure S3.** Flow pattern in the CFI at liquid to gas volumetric flow rate ratios of (a) 20, (b) 10, (c) 5 and (d) 2. Inlet concentration of H<sub>Au</sub>Cl<sub>4</sub> 0.27 mM.

**Table S1.** Representative length of gas bubble and liquid slug at different liquid to gas volumetric flow rate ratios.

| Liquid to gas flow rate ratio | Liquid slug length (mm) | Gas bubble length (mm) |
|-------------------------------|-------------------------|------------------------|
| 20                            | 7.1                     | 0.7                    |
| 10                            | 4.0                     | 0.9                    |
| 5                             | 2.9                     | 1.1                    |
| 2                             | 1.0                     | 0.9                    |

In Taylor flow the mass transfer occurs by two paths, from the hemispherical bubble cap to the surrounding liquid and from the film surrounding the bubble.<sup>2</sup> However, the flow pattern in Figure S3 showed convex liquid slugs due to the hydrophobic FEP tubing, indicating the absence of a liquid film surrounding the gas bubble. Hence, the overall mass transfer coefficient is equivalent to the cap mass transfer coefficient, which was calculated via:

$$k_{L,cap} = 2\sqrt{2\frac{D_{CO}V_b}{\pi^2 d_c}} \quad (S1)$$

where  $D_{CO} = 2 \times 10^{-9}$  m<sup>2</sup>/s is the liquid phase diffusivity of CO at 293 K,<sup>3</sup>  $V_b$  is the Taylor bubble velocity (calculated based on residence time and the length of the CFI) and  $d_c$  is the capillary tube diameter.

The volumetric mass transfer coefficient,  $k_{L,cap}a_{cap}$  was obtained by multiplying Eq. (S1) with the specific interfacial area for the two hemispherical caps:

$$a_{cap} = \frac{4}{L_{UC}} \quad (S2)$$

where the  $L_{UC}$  is the unit cell length (one gas bubble length + liquid slug length). The volumetric mass transfer coefficients calculated increase with decreasing liquid to gas volumetric flow rate ratio, as shown in Table S2.

**Table S2.** Calculated volumetric mass transfer coefficients.

| Liquid to gas flow rate ratio | $k_{L,cap} \times 10^4$ (m/s) | $a_{cap}$ ( $m^2/m^3$ ) | $k_{L,cap}a_{cap}$ ( $s^{-1}$ ) |
|-------------------------------|-------------------------------|-------------------------|---------------------------------|
| 20                            | 1.40                          | 511                     | 0.071                           |
| 10                            | 1.50                          | 810                     | 0.12                            |
| 5                             | 1.52                          | 982                     | 0.15                            |
| 2                             | 1.70                          | 2114                    | 0.36                            |

The above calculations are estimations based on straight tube; the secondary flow profile (Dean vortices) induced by centrifugal force and inversions with 90° bends<sup>4</sup> in the CFI were not taken into account. The Dean number ( $N_{De}$ ) for the liquid phase could be calculated by:

$$N_{De} = N_{Re} / \sqrt{\lambda} ; N_{Re} = d_c u \rho / \mu ; \lambda = D_{coil} / d_c \quad (S3)$$

where  $N_{Re}$  is the Reynolds number,  $u$  is the superficial liquid velocity,  $\rho$  is the liquid density,  $\mu$  is the liquid viscosity,  $\lambda$  is the curvature ratio and  $D_{coil}$  is the coil diameter. The Dean number of the liquid phase was 3.76, which is large enough to reduce axial dispersion by inducing chaotic mixing at the bends.<sup>5</sup> Thus, we expect the mass transfer in our reactor to be better than the estimation shown in Table S2, due to the radial convective transfer intensification by the CFI.<sup>6</sup>

#### 4. Characterization of gold nanoparticles synthesized via CO reduction

The particle size and size distribution of 0.030 mM and 0.54 mM inlet concentration of  $\text{HAuCl}_4$  in Figure 2 were obtained from TEM (Figure S4) and DCS (Figure S5) respectively.

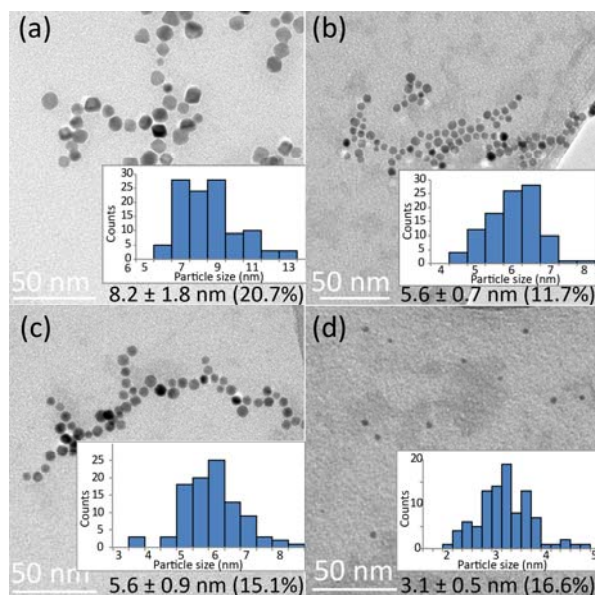


**Figure S4.** TEM images of gold nanoparticles at liquid to gas volumetric flow rate ratios of (a) 20, (b) 10, (c) 5 and (d) 2. Inlet concentration of  $\text{HAuCl}_4$  0.030 mM, synthesis at room temperature and residence time 3-5 min. Size of gold nanoparticles is shown along with standard deviation and polydispersity.

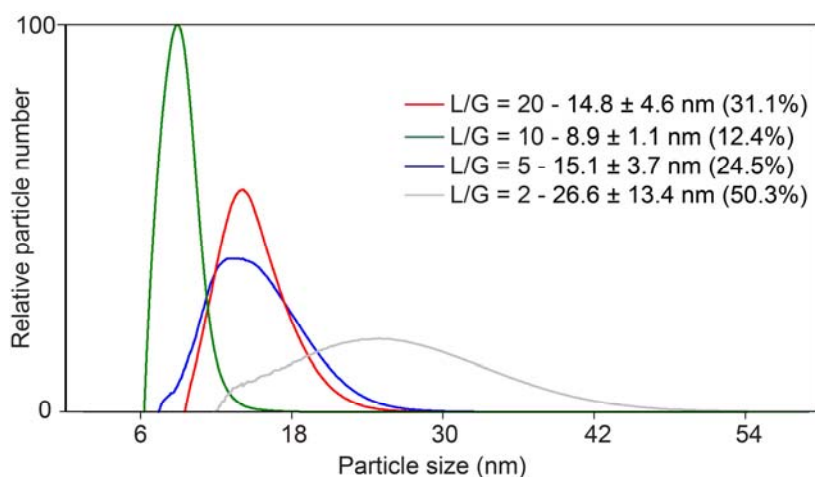


**Figure S5.** Particle size and size distribution of gold nanoparticles obtained from DCS (normalised by area in each curve) for samples obtained at liquid to gas volumetric flow rate ratios (L/G) of 20, 10, 5 and 2. Inlet concentration of  $\text{HAuCl}_4$  0.54 mM, synthesis at room temperature and residence time 3-5 min. Size of gold nanoparticles is shown along with standard deviation and polydispersity.

Figure S6 shows the IR spectra of CO-produced gold nanoparticles in aqueous solution. If the CO adsorbed on the gold surface, there should be a weak band around  $2125\text{ cm}^{-1}$ .<sup>7</sup> Its absence in Figure S6 indicated that no CO was present on the nanoparticles.

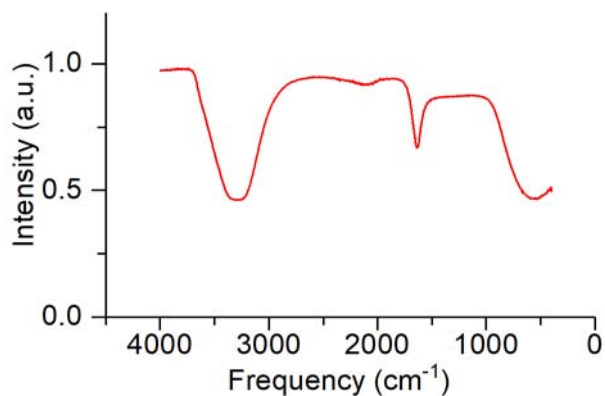


**Figure S6.** IR spectra of CO-produced gold nanoparticles in aqueous solution at inlet concentration of  $\text{HAuCl}_4$  0.54 mM, liquid to gas volumetric flow rate ratio 20, room temperature and residence time 5 min.

## 5. Calculation of SERS enhancement factor

SERS enhancement factors for analyte ( $EF$ ) were calculated using equations (S4), (S5) and (S6):

$$EF = I_{SERS} \times N_{bulk} / (I_{RS} \times N_{SERS}) \quad (S4)$$

$I_{SERS}$ : intensity of the band in SERS

$I_{RS}$ : intensity of the band in Raman spectra

$N_{bulk}$ : number of molecules probed in Raman sample

$N_{SERS}$ : number of molecules probed in SERS

For all spectra, baselines were corrected to get peak intensity. The laser spot size was measured in two dimensions of the substrate and was  $\approx 4.4 \mu\text{m}^2$ .

$$N_{SERS} = C_{SERS} V_{SERS} N_A A_{Raman} / A_{sub} \quad (S5)$$

$$N_{bulk} = \rho h N_A A_{Raman} / M \quad (S6)$$

$C_{SERS}$ : analyte solution molar concentration =  $4 \times 10^{-6}$  M ( $10^{-5}$  M of Rh6G solution mixed with gold colloidal solution at volume ratio of 2 : 3)

$V_{SERS}$ : volume of the droplet on substrate = 100  $\mu\text{L}$  in SERS

$N_A$ : Avogadro constant =  $6.02 \times 10^{23} \text{ mol}^{-1}$

$A_{Raman}$ : area of Raman scanning (i.e., Raman spot size) =  $4.4 \times 10^{-8} \text{ cm}^2$

$A_{sub}$ : area of the substrate =  $0.64 \text{ cm}^2$

$M$ : molecular weight =  $479.01 \text{ g mol}^{-1}$

$\rho$ : density =  $1.15 \text{ g cm}^{-3}$

$h$ : confocal depth =  $21 \mu\text{m}$

The above values give

$$N_{SERS} = 4 \times 10^{-6} \times 10^{-4} \times 6.02 \times 10^{23} \times 4.4 \times 10^{-8} / 0.64 = 1.66 \times 10^7 \text{ molecules}$$

$$N_{bulk} = 1.15 \times 0.0021 \times 6.02 \times 10^{23} \times 4.4 \times 10^{-8} / 479.01 = 1.34 \times 10^{11} \text{ molecules}$$

Three peaks were chosen to calculate the enhancement factor as shown in Table S3.

**Table S3.** SERS enhancement factor of gold nanoparticles solutions.

| Wavenumber                        | Band intensity           |        |        |        |        | Enhancement factor, EF |                    |                    |                    |
|-----------------------------------|--------------------------|--------|--------|--------|--------|------------------------|--------------------|--------------------|--------------------|
|                                   | Raman_R<br>h6G<br>powder | SERS_A | SERS_B | SERS_C | SERS_D | SERS_A                 | SERS_B             | SERS_C             | SERS_D             |
| <b>611 cm<sup>-1</sup></b>        | 1137                     | 3752   | 9291   | 12516  | 17997  | $2.66 \times 10^4$     | $6.60 \times 10^4$ | $8.89 \times 10^4$ | $1.28 \times 10^5$ |
| <b>1359 cm<sup>-1</sup></b>       | 1097                     | 4509   | 16084  | 32196  | 26588  | $3.32 \times 10^4$     | $1.18 \times 10^5$ | $2.37 \times 10^5$ | $1.96 \times 10^5$ |
| <b>1509 cm<sup>-1</sup></b>       | 1070                     | 3956   | 17672  | 33952  | 27540  | $2.98 \times 10^4$     | $1.33 \times 10^5$ | $2.56 \times 10^5$ | $2.08 \times 10^5$ |
| <b>Average enhancement factor</b> |                          |        |        |        |        | $2.99 \times 10^4$     | $1.06 \times 10^5$ | $1.94 \times 10^5$ | $1.77 \times 10^5$ |

SERS\_A: Commercial citrate-capped 10 nm gold nanoparticles

SERS\_B: CO-produced 7.7 nm gold nanoparticles synthesized in this work

SERS\_C: CO-produced 26.6 nm gold nanoparticles synthesized in this work

SERS\_D: Commercial citrate-capped 30 nm gold nanoparticles

## 6. Synthesis procedures of gold nanoparticles with different capping agents

### 6.1 Citrate-capped gold nanoparticles

As the gold nanoparticles obtained were positively charged, adding trisodium citrate after synthesis led to immediate aggregation. Thus, the citrate solution (0.54 mM) was mixed with H<sub>2</sub>AuCl<sub>4</sub> solution (0.54 mM) via a micromixer chip (Dolomite, Part No. 3000144) before mixing with CO via the T-junction at room temperature. The residence time was 4.4 min with the volumetric flow rates of CO set at 0.05 ml/min, and both citrate and gold precursor flow rates were 0.25 ml/min.

### 6.2 TWEEN 80-capped gold nanoparticles

0.27 mM polysorbate 80 (TWEEN 80) solution was mixed with H<sub>2</sub>AuCl<sub>4</sub> solution (0.54 mM) with the same flow rate of 0.25 ml/min using the micromixer chip, before forming segmented flow with CO (0.1 ml/min) in the CFI. TWEEN 80 acts as a capping agent<sup>8</sup> and hence can suppress the reduction rate.<sup>9</sup> Thus, the reaction continued in the collection container, as monitored by UV-Vis. The particle size increased from  $2.7 \pm 0.4$  nm (14.6%) (see Figure S7c) to  $4.0 \pm 0.4$  nm (9.9%) (see Figure 5b) over a period of 8 days. The polydispersity decreased after 8 days, as the TWEEN 80 could also act as a weak reducing agent for seed-mediated growth.<sup>10</sup> This suggests that the CO reduction inside the CFI formed a high amount of seed particles without consuming the entire gold precursor. The remaining TWEEN 80 subsequently reduced the precursor with a size-focusing effect<sup>11</sup> to form monodisperse particles.

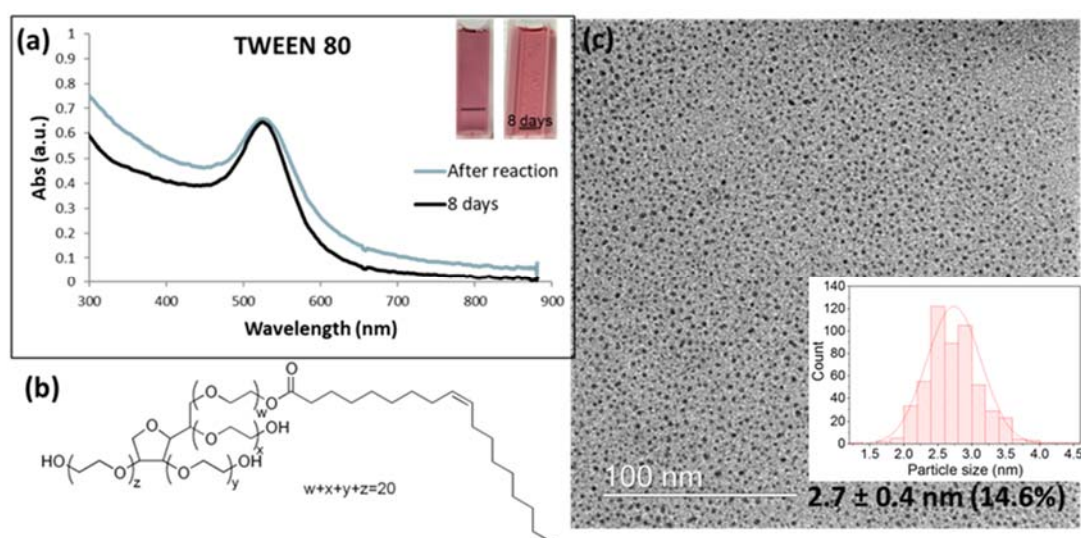


**Figure S7.** (a) UV-Vis spectra of fresh gold nanoparticles capped by TWEEN 80 obtained at the outlet of the CFI and after 8 days storage (insert shows the colour of the samples); (b) the structure of TWEEN 80; (c) TEM image of fresh gold nanoparticles capped by TWEEN 80 obtained at the outlet of the CFI. Corresponding average size and polydispersity of synthesized gold nanoparticles obtained by TEM are also shown.

### 6.3 Oleylamine-capped gold nanoparticles

The proposed synthesis was able to produce oleylamine-capped hydrophobic gold nanoparticles. The final concentration of 0.27 mM H<sub>2</sub>AuCl<sub>4</sub> solution was obtained by dissolving solid gold(III) chloride trihydrate into octane solution containing 0.54 mM oleylamine. This gold solution was reduced by CO (0.1 ml/min) in the microfluidic segmented system at 100°C,

placed in a stirred glycerol (99.5%, VWR) bath on a hot plate (Stuart, UC152D with SCT temperature controller) with residence time of 4.2 min and liquid to gas volumetric flow rate ratio of 5. The synthesized gold nanoparticles were precipitated by acetone and then centrifuged at 6000 rpm (Heraeus Multifuge X1R, ThermoFisher) for 30 min. The precipitated gold nanoparticles were re-dispersed in toluene for TEM sample preparation.

An experiment was performed where N<sub>2</sub> was used to replace CO at the same experimental conditions to investigate if the CO was the dominant reducing agent rather than oleylamine. Figure S8 shows that single-crystal nanowires were formed without CO, similar to previous literature<sup>12</sup> that showed nanowire production by oleylamine reduction.

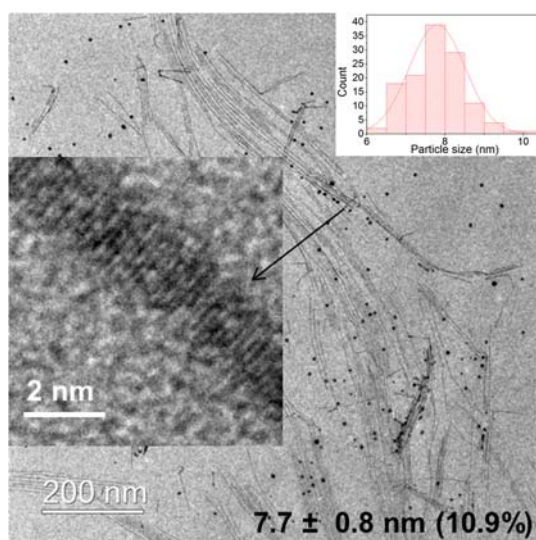


**Figure S8.** TEM image of gold nanoparticles in oleylamine-only reduction without CO. The product contained a mixture of spherical gold nanoparticles ( $7.7 \pm 0.8$  nm, 10.9%) and Au nanowires ( $\sim 1.7$  nm in width and few  $\mu\text{m}$  in length). Insert shows the nanowire lattice.

#### 6.4 Thiol-PEG-COOH capped gold nanoparticles

For the synthesis of thiol-PEG-COOH capped gold nanoparticles, firstly 0.3% w/w poly(sodium 4-styrenesulfonate) (PSS) was mixed with 0.27 mM HAuCl<sub>4</sub> solution via a micromixer chip with the same flow rate of 0.125 ml/min and then reacted with CO (0.1 ml/min) in the CFI with residence time of 7.5 min. The synthesized gold nanoparticles (which were capped with PSS) were characterized by UV-Vis and TEM (see Figure S9). At 5 ml product collected from the reactor, 5 ml poly(ethyleneglycol) 2-mercaptoethyl ether acetic acid solution (MW = 3163 Dalton, 100  $\mu\text{g}/\text{ml}$ ) (Thiol-PEG-COOH) was added with stirring overnight at room temperature to replace the PSS. After the thiol-PEG-COOH replacement, the particle size did not change (average particle size of 7.8 nm in Figure 5d), indicating that the gold nanoparticles were stable after the ligand exchange.

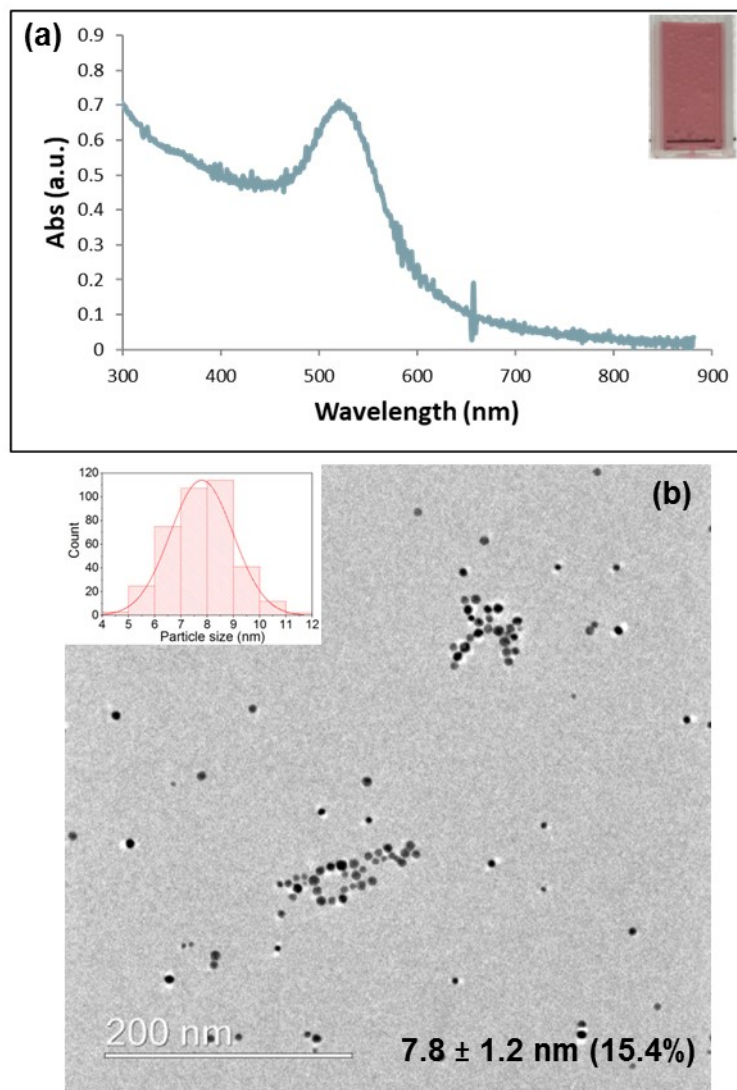


**Figure S9.** (a) UV-Vis spectra of fresh gold nanoparticles capped by PSS (insert shows the colour of the sample); (b) TEM image of gold nanoparticles capped by PSS.

## References

1. Angeli, P.; Gavriilidis, A., Taylor flow in microchannels. In *Encyclopedia of Microfluidics and Nanofluidics*, Springer: New York, 2008; pp 1971-1976.
2. Van Baten, J.; Krishna, R., CFD simulations of mass transfer from Taylor bubbles rising in circular capillaries. *Chem Eng Sci* **2004**, *59* (12), 2535-2545.
3. Wise, D.; Houghton, G., Diffusion coefficients of neon, krypton, xenon, carbon monoxide and nitric oxide in water at 10–60 °C. *Chem Eng Sci* **1968**, *23* (10), 1211-1216.
4. Kurt, S. K.; Warnebold, F.; Nigam, K. D.; Kockmann, N., Gas-liquid reaction and mass transfer in microstructured coiled flow inverter. *Chem Eng Sci* **2017**, *169*, 164-178.
5. Rossi, D.; Gargiulo, L.; Valitov, G.; Gavriilidis, A.; Mazzei, L., Experimental characterization of axial dispersion in coiled flow inverters. *Chemical Engineering Research and Design* **2017**, *120*, 159-170.
6. Vashisth, S.; Nigam, K., Experimental investigation of void fraction and flow patterns in coiled flow inverter. *Chemical Engineering and Processing: Process Intensification* **2008**, *47* (8), 1281-1291.
7. Zhang, T.; Driver, S. M.; Pratt, S. J.; Jenkins, S. J.; King, D. A., Ir-induced activation of Au towards CO adsorption: Ir films deposited on Au {111}. *Surface Science* **2016**, *648*, 10-13.
8. Zhao, Y.; Wang, Z.; Zhang, W.; Jiang, X., Adsorbed Tween 80 is unique in its ability to improve the stability of gold nanoparticles in solutions of biomolecules. *Nanoscale* **2010**, *2* (10), 2114-2119.
9. Campisi, S.; Schiavoni, M.; Chan-Thaw, C. E.; Villa, A., Untangling the role of the capping agent in nanocatalysis: Recent advances and perspectives. *Catalysts* **2016**, *6* (12), 185.
10. Premkumar, T.; Kim, D.; Lee, K.; Geckeler, K. E., Polysorbate 80 as a tool: Synthesis of gold nanoparticles. *Macromolecular Rapid Communications* **2007**, *28* (7), 888-893.
11. Jana, N. R.; Gearheart, L.; Murphy, C. J., Seeding growth for size control of 5–40 nm diameter gold nanoparticles. *Langmuir* **2001**, *17* (22), 6782-6786.
12. Feng, H.; Yang, Y.; You, Y.; Li, G.; Guo, J.; Yu, T.; Shen, Z.; Wu, T.; Xing, B., Simple and rapid synthesis of ultrathin gold nanowires, their self-assembly and application in surface-enhanced Raman scattering. *Chem. Commun.* **2009**, (15), 1984-1986.